Multilayer Perceptron to Boost Colorimetric Capacities of 2D RGB and Hyperspectral Snapshot Cameras

Eric Lopez-Lopez
Robotics and Control Unit
AIMEN Technology Centre
Porriño, Spain
https://orcid.org/0000-0002-7720-1607

Roi Mendez-Rial
Robotics and Control Unit
AIMEN Technology Centre
Porriño, Spain
https://orcid.org/0000-0002-9991-0316

***Abstract*—The ability to accurately measure the surface colour has enormous applications in the quality control of a wide range of manufacturing processes. Currently, the industry still relies on traditional colourimeters to implement these tasks.**

In this work, we compare the behaviour of two types of snapshot cameras (RGB and hyperspectral) in the frame of accurate colour measuring. We use two approaches for colour and spectral reconstruction, one based on linear modelling and another novel one based on Multilayer Perceptron (MLP). Experiments use charts with a large number of different colours (165 for training and 165 for testing). The results showed promising properties of neural networks in this task. We reach an average 1.6 CIEDE 2000 colour difference between estimations and ground truth.

***Index Terms*—colorimetry, hyperspectral imaging, snapshot cameras, neural networks**

I. Introduction

The ease with which we perceive colours contrasts with the difficulty to explain its nature [1]. In general terms, we can say that colour is the representation of a specific light spectrum in the mind. During the last decades, colour scientists have put enormous efforts to model how humans perceive colours. Apart from the unequivocal theoretical interest, these efforts have been also driven for the enormous applications of accurate colour representations for quality control in the industry (e.g. textiles [2], foods [3]–[5], woodworking [6], automotive [7], etc.).

Currently, the most reliable solution to systematically measure the colour of a surface is to rely on colourimeters [8]. Nevertheless, its contrasted accuracy comes with some limitations like issues relating to measure non-flat surfaces or the inability to measure many colours at the same time [9]. Alternatively, camera-based approaches appear as a solution to this problems [8], [10]. The setup used by most of these approaches generally requires a controlled illumination environment. Therefore, RGB cameras are usually used in combination with light cabinets [11]. Nevertheless, the accurcy of these setups still suffer a non-neglectable degradation with respect to colourimeters.

This work was supported by the European Union's Horizon 2020 research and innovation programme through MULTIPLE project under grant agreement No 871783.

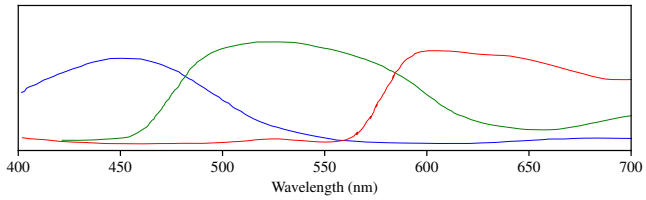

(a) RGB Camera

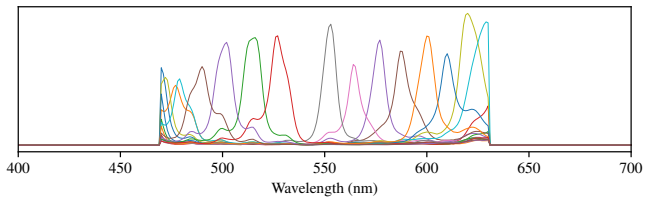

(b) Snapshot Visible Hyperespectral Camera

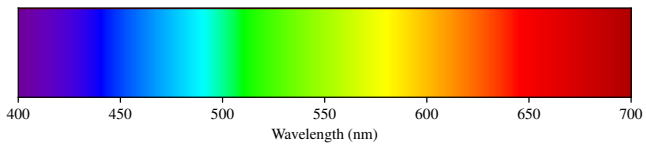

(c) Visible spectrum

Fig. 1: Spectral sensitivity of the sensors present in the hyperespectral and the regular RGB cameras used during the experiments.

One possible option for closing this gap is to substitute RGB cameras with hyperspectral ones. Hyperspectral images (HSI) generalise this *tri-sensor* architecture of traditional RGB cameras in terms of both number and types, bringing an entirely new dimension into the imaging acquisition and spectral reconstruction task. This way, the hybrid nature between regular imaging and spectroscopy [12] makes the use of HSI

especially interesting for colour and spectral reconstruction. For instance, a set of sensors with a very narrow wavelength response could densely sample the original spectra and so potentially improve the accuracy of the reconstruction of both spectrum and colour (see Fig. 1).

There is a wide variety of imaging techniques for HSI cameras. Nevertheless, for colourimeter-alike real-time colour measuring, snapshot cameras are the more appropriate [13]. The strategy followed by these cameras generalise the traditional 2×2 RGB Bayer Filter Array tile to an $n \times n$ tile to acquire the hypersepectral image at once. Notwithstanding their benefits in terms of usability or quickness come with new challenges like the demosaicing artefacts or sensor non-uniformity issues [13].

In regards to the methods which are often used to perform this colour reconstruction, most of them rely on either linear, quadratic models [8], or one layer neural networks [14]. Recently, a Multilayer Perceptron (MLP) have been successfully proposed for colour reconstruction in an HSI-alike setup [15] and in simulated scenarios with RGB [16]. Up to our knowledge, there is an absence of works which analyse the performance of MLP in colour reconstruction tasks with real-world images of both RGB and HSI cameras.

In this setting, this paper makes the following contributions:

- A method based on artificial neural networks to boost colour fidelity.
- The study of the viability of state-of-the-art snapshot hyperspectral cameras in comparison with traditional RGB cameras for colorimetric purposes with real-world images.

The rest of the paper is organised as follows. Firstly, we will explain and formulate the problem we are going to tackle (Sec. II). After that, we will move on to describe the experimental setup (Sec. III). Finally, we will show the achieved results (Sec. IV) and the conclusions which can be extracted from the work (Sec. V).

II. Problem Formulation

For clarity purposes, the scope of the work is restricted to the reflective case. Thus, an imaging process can be modelled as a function, $\mathbf{f}(\cdot)$, dependent on the raw spectral reflectance of the surface (i.e. surface colour). This function would also be dependent on the type of illumination and the type of sensor of the imaging system. Nevertheless, since the objective is to infer the spectral reflectance, the last two variables are usually fixed in the experiments. This way, the pixel value will only be dependent on the spectral reflectance:

$$\mathbf{p} = \mathbf{f}(\mathbf{r})$$

where $\mathbf{p}$ are n-dimensional vectors (n types of sensor) with the sensor responses (i.e. pixel values) and $\mathbf{r}$ are m-dimensional vectors containing the spectral reflectance (m refers to the discretisation of the spectrum or the number of colour coordinates).

TABLE I: Number of nodes per layer of the MLP used for colour and spectral reconstructions.

Layer	Colour		Spectrum		Activation
	RGB	HSI	RGB	HSI	Function
Input Layer	3	16	3	16	
1st Layer	128		128		ReLu
2nd Layer	64		64		ReLu
Output Layer	3		43		Linear

Here, on one hand, $n = 3$ for the RGB camera and $n = 16$ for the HSI one. On the other hand, $m = 43$ for the spectral reconstruction task (43 bins of 10 nm between 360 and 780 nm) and $m = 3$ colour coordinates for the colour reconstruction task.

Aiming to infer the actual spectral reflectance based on $\mathbf{p}$, we need to compute the inverse of the function $\mathbf{f}$, such as:

$$\mathbf{r} = \mathbf{f}^{-1}(\mathbf{p}) = \mathbf{g}(\mathbf{p}) \tag{1}$$

In practice, instead of working with raw spectra, it is common to work with colours. For this purpose, the CIE XYZ colour system is defined, which transforms the spectra into tristimuli values using a linear transformation C (a $3 \times m$ matrix) [17]:

$$\mathbf{C} \cdot \mathbf{r} = \mathbf{C} \cdot \mathbf{g}(\mathbf{p}) \Rightarrow$$

$$\mathbf{r}_{XYZ} = \mathbf{g}_{XYZ}(\mathbf{p}) \tag{2}$$

where $\mathbf{r}_{XYZ}$ is 3-dimensional. The quality of the function $\mathbf{g}$ or $\mathbf{g}_{XYZ}$ will measure the spectral or colourimetric accuracy of the camera, respectively.

We will use two methods to estimate $\mathbf{g}$: using a linear estimation (Sec. II-A) or with an Multilayer Perceptron (Sec. II-B).

A. Linear Estimation

The assumption of $\mathbf{g}$ to be a linear function is something common in previous works [8] and is justified by physical models [18]. This way, (1) and (2) expressions become:

$$\mathbf{r} = \mathbf{M} \cdot \mathbf{p}$$

$$\mathbf{r}_{XYZ} = \mathbf{M}_{\mathbf{XYZ}} \cdot \mathbf{p}$$

where $\mathbf{M}$ is a $m \times n$ matrix and $\mathbf{M}_{XYZ}$ is a $3 \times n$.

Therefore, having k pairs of sensors responses for known spectral reflectances, we can estimate the $\mathbf{M}$ using the pseudo-inverse [18]:

$$\mathbf{M} = \mathbf{r}^T \cdot \mathbf{p} \cdot \left(\mathbf{p}^T \cdot \mathbf{p}\right)^{-1}$$

An analogous procedure can be performed to instead of reconstruction spectra, reconstruct the CIE XYZ colour coordinates (with $\mathbf{r}_{XYZ}$ and $\mathbf{M}_{XYZ}$).

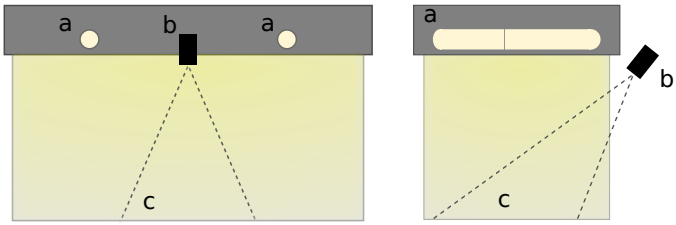

Fig. 2: Front and lateral views of the acquisition equipment. The light cabin is illuminated using the standard D65 lights (a). The camera (b) is located in the middle of the top part outside the cabin, providing for a field of view (c) of approximately 20×15 cm.

B. Multilayer Perceptron

Artificial Neural Networks (ANN) allow the estimation of the function $\mathbf{g}$ without any assumption on its nature. Inspired by [15], we chose to use a 2-layer Multilayer Perceptron (MLP) to fit the pairs of sensor responses and known colour/spectral reflectance in a regression fashion. The number of nodes in each layer (Tab. I) was determined experimentally.

We selected the Mean Squared Error (MSE) as loss function:

$$\mathcal{L} = \frac{1}{m}\sum_{i=1}^{m}\left(r_i - g_i\left(\mathbf{p}\right)\right)^2$$

Here, r_i is the ith-component of the pixel ground truth and g_i is the ith-component of the estimation. Finally, m will be 3 for colour estimations and 43 for spectral estimations.

Nevertheless, since we do not need to make assumptions about $\mathbf{g}$, we opted to use the CIELAB or L*a*b* colour system [19] in colour reconstructions due to its preferable properties in terms of colour uniformity with respect to human perception. Besides, this way the MSE loss function would be similar to the CIE76 colour difference convention. All of this means that the optimisation process will minimise differences in colour in a similar way as they are perceived by humans. We have used the Adam optimiser during the training process.

III. Experimental Setup

The experimental setup consists of three main elements. First, the RGB and HSI cameras acquire the image information for colour reconstruction. Second, a light cabinet with a controlled illumination environment. Finally, an object with known colour coordinates and spectral reflectances to fit and test our estimation models.

In the following subsections, we will be providing a detailed explanation of each element jointly with the pre-processing procedures and metrics we have utilised.

A. Cameras and illumination

The experiments have been performed using two different snapshot cameras taken from the machine vision scope:

- The RGB camera is a Teledyne Dalsa Genie Nano C2420 Color. This camera possesses a Sony IMX264 sensor with the traditional Bayer Colour Filter Array, a resolution of $2\,448 \times 2\,048$ and capable of reaching 23.80 fps. Sensitivity over the visible spectrum of each of the three different sensors can be seen in Fig. 1a.
- The snapshot hyperspectral camera is a Photon Focus MV1-D2048x1088-HS03-96-G2. The sensor is an IMEC CMV2K-SSM4X4-VIS, with a resolution of 2048×1088 pixels. This sensor has the particularity of having an array of filters which allows capturing the hyperspectral data. Filters are disposed in 4×4 tiles (i.e. a total of 16 different bands), with each element of the tile focused in a different region of the spectra between 470 nm and 620 nm (see Fig. 1b). This design allows for a quick acquisition time of up to 42 fps, something hard to achieve with other hyperspectral architectures.

In regards to the lens setup, we opted to use a 35 mm lens with both cameras. This way we maximise the field of view without having vignetting problems. This is something especially relevant since we are developing pixel-level colour estimation models (Sec. II) without taking into account any spatial information. Therefore, it is important to have a response as uniform as possible over the frame.

Finally, in regards to the illumination, we wanted to have fixed and controlled illumination environment to be able to not take into account the influence of the illumination spectra in the colour estimation model (see Sec. II). In this sense, the experiments were performed in a light cabin with a controlled standard D65 illumination. This type of light cabin is widely used in colourimetric applications. The camera was located out of the cabin to avoid any glare. Fig. 2 shows a scheme of the whole setup.

B. Dataset Generation

For both the generation of the colour calibration models of Sec. II and for testing purposes, we need some physical objects with known spectral reflectance and colour coordinates under a certain illumination. For this purpose, we were inspired by [15] to use a printed version ECI 2002 CYMK chart [20]. Since it is difficult to control how these colours will exactly be printed, we decided to use a colourimeter (the Xrite Ci64-XR) to measure the reflectance spectrum and L*a*b* colour coordinates of each patch, generating the ground truth. We assume that the colour of each patch is uniform.

The ECI 2002 CYMK contains 1485 patches of colours and is widely used as a target for printers' colour calibration. Given the large number of colour patches available, we opted to print just two random sub-samplings of the complete set (taking 2 out 9 colours of the set) to create the so-called *Chart A* and *Chart B* (see Fig. 3), each of them with 165 colours and no common ones between them. This way we increase the surface available of each patch to make them readable by the colourimeter and, at the same time, we keep the size of the chart small enough to fit it in the camera's field of view. We have made publicly available both the HSI and RGB raw images and the colourimeter data [21].

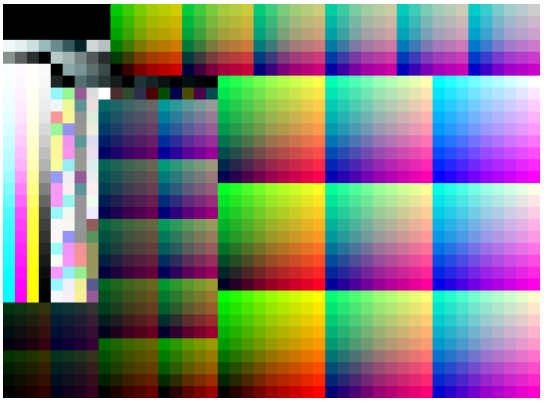

(a) Original ECI2002 target.

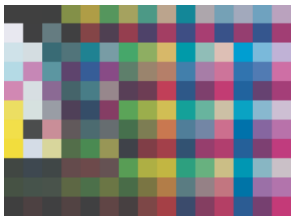

(b) Effective colours of the first printed subset (Chart A)

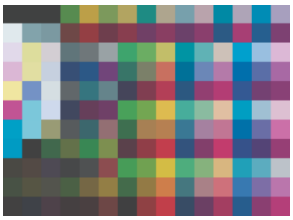

(c) Effective colours of the second printed subset (Chart b)

Fig. 3: The original ECI2002 target, and the two different subsets (of 15x11 colours) used during the experiments. (a) shows the original digital color values of the chart, (b) and (c) show the effective colour after printing, measured by the colorimeter.

The idea is to use one of the charts to fit our models (*Chart A*) and the other for evaluation purposes (*Chart B*). To do so, we have extracted pixels containing about 70-80% of the patches surface as probes.

C. Pre-processing

During the image acquisition phase, we performed three (four with MLP) main procedures to pre-process raw camera data:

1) *Demosaicing.* Since this work is centred around snapshot cameras, each pixel of the array will only measure information with one sensor. Therefore, it is necessary to infer the value of the other sensors. Here, we opted to use the common weighted bi-linear estimation [22].
2) *Denoising.* The pixel-level estimation of this work forces us to optimise the responses' uniformity along with the sensor array. For this reason, each image acquisition is an average of 10 images to reduce pixel noise.
3) *White-dark normalisation.* For the same uniformity reasons as above, we have taken images of both black (I_{ij}^{dark}), and white (I_{ij}^{white}) surfaces. Then, we perform this transformation to the original image:

$$\hat{I}_{ij} = \frac{I_{ij} - I_{ij}^{\text{dark}}}{I_{ij}^{\text{white}}}$$

This way, we minimise the effect of the different dynamic ranges of each sensor type.
4) *Standardisation.* This pre-processing will only be performed for the MLP fitting. It consist of normalising data to align it with a normal distribution. This transformation has proven to help in the numerical convergence of the neural networks training phase [23].

TABLE II: Median and average values of ΔE_{00} between the estimation and ground truth for each tested method. MLP methods are averaged over multiple runs to address the randomness of the training process.

Method	Min	Median	Average	Max
RGB+LT	0.0070	2.260	2.627	21.030
HSI+LT	0.0155	2.103	2.530	19.517
RGB+MLP	0.0074	**1.249**	**1.572**	19.834
HSI+MLP	0.0130	1.454	1.700	19.813

D. Metrics

Performance evaluation of the colour estimations in comparison to the ground truth will be assessed using CIEDE 2000 colour difference (ΔE_{00}) [24]. This is the most advanced colour difference metric convention in relation to how humans perceive colours.

In regards to the spectral reflectance reconstruction, we will use the standard Mean Squared Error (MSE) between estimations and ground truth:

$$MSE = \frac{1}{m}\sum_{i=1}^{m}(r_i - g_i)^2$$

where r_i is the ith-component of the pixel ground truth and g_i is the ith-component of the estimation. Finally, m will be 3 for colour estimations and 43 for spectral estimations.

Finally, it is important to notice that MLP evaluation metrics will be averaged over 10 different runs. The stochastic nature of the training of neural networks provokes some variability in the specific results.

IV. Results

This section presents the results achieved for colour (Sec. IV-A) and spectral reflectance (Sec. IV-B) estimations.

A. Colour coordinate estimation

The average, median, minimum and maximum colour differences respect to the evaluation chart (*Chart B*) can be seen in Tab. II. Besides, the distribution of ΔE_{00} values can be also observed on the *Violin plot* in Fig. 4. The first thing we extract from the results is the evident push in the performance of MLP estimation. There is almost a ΔE_{00} of 1 between both types of estimations. These lower ΔE_{00} can also be observed in the reconstructions presented on Fig. 5.

Comparing now Hyperspectral Imaging (HSI) respect to regular RGB images, the results shows better behaviour of HSI with the linear estimation. Nevertheless, this advantage do not translate to the MLP estimation, meaning that the combination

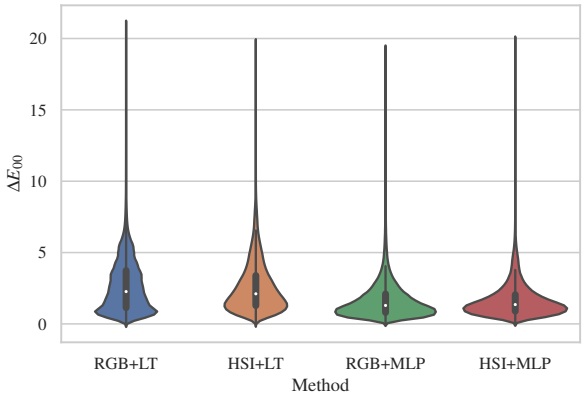

Fig. 4: Violin plot of the distribution of ΔE_{00} between prediction and ground truth, for one of the runs. The white dot represent the median, the wider line represent the interquartile range, and the slimer centre line represent 1.5 times the interquartile range.

TABLE III: Average absolute differences of each L*a*b* coordinate between the estimation and the ground truth. MLP methods are averaged over multiple runs to address the randomness of the training process.

Method	ΔL*	Δa*	Δb*
RGB+LT	0.640	3.228	1.662
HSI+LT	1.102	1.419	3.296
RGB+MLP	**0.506**	1.343	**1.363**
HSI+MLP	0.612	**0.953**	1.582

of RGB+MLP is the one which is able to achieve the best colour reconstruction.

Tab. III shows a bit more insight into the reasons for this behaviour. This table contains the differences in each L*a*b* coordinate with respect to the ground truth. Taking into account the meaning of each of the coordinates (L* = lightness, a* = green-red, b* = blue-yellow), we can extract some valuable information. While RGB cameras present the largest differences a* coordinate, HSI tends to do so with b*. Looking at the previous Fig. 1, we see that the HSI camera leaves out a great part of the blue spectrum, while in the red region only the darker part is missing. Therefore, the greater values of Δa* for HSI are explained by the fact that the camera is not sensitive to this part of the spectrum.

B. Spectral reflectance reconstruction

The end of the previous section suggests that the quality of the spectral reflectance reconstruction depends on the region of the spectra. Therefore, this section serves to perform further analysis of this hypothesis. We fitted both models (linear and MLP) to the spectral data acquired with the colourimeter to see if there are regions which are being reconstructed better than others. Our main interest is to compare the quality of the reconstructions (MSE with respect to the ground truth) in the

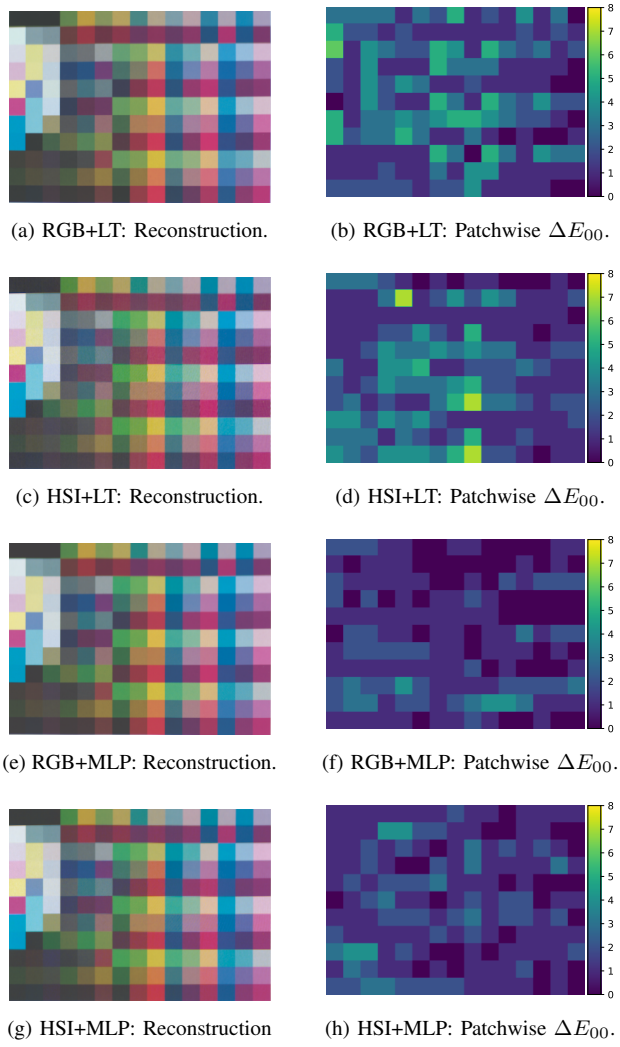

(a) RGB+LT: Reconstruction. (b) RGB+LT: Patchwise ΔE_{00}.

(c) HSI+LT: Reconstruction. (d) HSI+LT: Patchwise ΔE_{00}.

(e) RGB+MLP: Reconstruction. (f) RGB+MLP: Patchwise ΔE_{00}.

(g) HSI+MLP: Reconstruction (h) HSI+MLP: Patchwise ΔE_{00}.

Fig. 5: Colour reconstruction with each tested method along with the correspondent ΔE_{00} in each patch.

TABLE IV: MSE between estimated and ground truth *inside* (between 470 and 620 nm) and *outside* (the rest of the spectrum) the HSI sensitive region. MLP methods are averaged over multiple runs to address the randomness of the training process.

Method	Inside	Outside	Full
RGB+LT	7.913	4.498	5.768
HSI+LT	1.984	5.586	4.246
RGB+MLP	1.036	**1.621**	**1.404**
HSI+MLP	**0.949**	1.762	1.462

region inside the sensitive region of the hyperspectral camera, and outside it. The results are presented in Tab. IV.

As expected, the hyperspectral camera performs a better reconstruction in comparison to the RGB camera inside the region between 470 nm and 620 nm. The opposite occurs for the rest of the spectra.

On the other hand, like the previous experiment, we can

also observe the better performance of MLP in comparison to the linear estimation.

V. Conclusions

This work has studied the potential applications of both RGB and snapshot HSI cameras for colourimetric applications with real-world images. We compare the behaviour of two different approaches to perform the colour and spectral reconstruction, the simple linear model widely used in the literature and a novel method based on neural networks.

The experiments clearly showed the benefits which MLP provides (about 1 unit improvement of ΔE_{00}) in the estimation of the colour coordinates of the object surfaces. The best performance was achieved by traditional RGB cameras and MLP reconstruction method. The analysis of the spectral reconstruction showed that the snapshot HSI camera is still penalised by the fact that it does not cover the complete visible spectrum. Nevertheless, this analysis also suggests that widening the coverage could effectively transform snapshot HSI cameras into a real-time 2D colourimeter.

Finally, this work also show that there still is a gap in the colourmetric accuracy between cameras and colourimeters. Nevertheless, cameras provide in exchange more spatial resolution and the ability to measure larger regions of the space. Therefore, they appear as a viable and interesting solution to automate quality control in manufacturing processes.

References

[1] J. Koenderink, *Color for the Sciences*. MIT Press, 2010.

[2] P. T. F. Chong, "Colorimetry for textile applications," in *Modern textile characterization methods*. CRC Press, 2017, pp. 355–391.

[3] F. Cairone, S. Carradori, M. Locatelli, M. A. Casadei, and S. Cesa, "Reflectance colorimetry: A mirror for food quality—a mini review," *European Food Research and Technology*, vol. 246, no. 2, pp. 259–272, 2020.

[4] K. Ratprakhon, W. Neubauer, K. Riehn, J. Fritsche, and S. Rohn, "Developing an automatic color determination procedure for the quality assessment of mangos (mangifera indica) using a ccd camera and color standards," *Foods*, vol. 9, no. 11, 2020.

[5] P. S. Minz and C. S. Saini, "Rgb camera-based image technique for color measurement of flavored milk," *Measurement: Food*, vol. 4, p. 100012, 2021.

[6] W. C. S. Sousa, L. d. J. Barbosa, A. A. V. Soares, S. L. Goulart, and T. d. P. Protásio, "Wood colorimetry for the characterization of amazonian tree species: A subsidy for a more efficient classification," *Cerne*, vol. 25, pp. 451–462, 2020.

[7] M. E. Nadal and T. A. Germer, "Colorimetric characterization of pearlescent coatings," in *9th Congress of the International Colour Association*, vol. 4421. International Society for Optics and Photonics, 2002, pp. 757–760.

[8] G. C. Guarnera, S. Bianco, and R. Schettini, "Turning a digital camera into an absolute 2d tele-colorimeter," *Computer Graphics Forum*, vol. 38, no. 1, pp. 73–86, 2019.

[9] M. Matusiak, "Digieye application in cotton colour measurement," *Autex Research Journal*, vol. 15, no. 2, pp. 77–86, 2015.

[10] P. Sanmartín, E. Chorro, D. Vázquez-Nion, F. M. Martínez-Verdú, and B. Prieto, "Conversion of a digital camera into a non-contact colorimeter for use in stone cultural heritage: The application case to spanish granites," *Measurement*, vol. 56, pp. 194–202, 2014.

[11] C.-N. Nguyen, V.-T. Vo, and N. Cong Ha, "Developing a computer vision system for real-time color measurement – a case study with color characterization of roasted rice," *Journal of Food Engineering*, vol. 316, p. 110821, 2022.

[12] A. Khan, M. Munir, W. Yu, and B. Young, "A review towards hyperspectral imaging for real-time quality control of food products with an illustrative case study of milk powder production," *Food and Bioprocess Technology*, vol. 13, p. 739–752, 05 2020.

[13] D. H. Foster and K. Amano, "Hyperspectral imaging in color vision research: tutorial," *JOSA A*, vol. 36, no. 4, pp. 606–627, 2019.

[14] K. León, D. Mery, F. Pedreschi, and J. León, "Color measurement in lab units from rgb digital images," *Food Research International*, vol. 39, no. 10, pp. 1084–1091, 2006, physical Properties VI.

[15] B. D. Batinić, M. S. Arbanas, J. S. Bajić, S. R. Dedijer, V. M. Rajs, N. M. Laković, and N. R. Kulundžić, "Using machine learning for improvement of reflected spectrum estimations of colorimetric probe," *IEEE Transactions on Instrumentation and Measurement*, vol. 70, pp. 1–7, 2021.

[16] L. MacDonald, "Color space transformation using neural networks," in *Color and Imaging Conference*, vol. 2019, no. 1. Society for Imaging Science and Technology, 2019, pp. 153–158.

[17] ASTM, "Practice for computing the colors of objects by using the CIE system," 2018.

[18] H.-L. Shen, P.-Q. Cai, S.-J. Shao, and J. H. Xin, "Reflectance reconstruction for multispectral imaging by adaptive wiener estimation," *Optics express*, vol. 15, no. 23, pp. 15 545–15 554, 2007.

[19] E. C. Carter, J. Schanda, R. Hirschler, S. Jost, M. R. Luo, M. Melgosa, Y. Ohno, M. R. Pointer, D. C. Rich, F. Viénot, L. Whitehead, and J. H. Wold, *CIE 015:2018 Colorimetry*. International Commission on Illumination, 2018.

[20] E. C. I. (ECI). (2002) Eci 2002 target. [Online]. Available: http://www.eci.org/

[21] E. Lopez-Lopez and R. Mendez-Rial, "AIMEN Colour Chart Dataset," Jul. 2022. [Online]. Available: https://doi.org/10.5281/zenodo.6586611

[22] S. Mihoubi, O. Losson, B. Mathon, and L. Macaire, "Multispectral demosaicing using pseudo-panchromatic image," *IEEE Transactions on Computational Imaging*, vol. 3, no. 4, pp. 982–995, 2017.

[23] Y. A. LeCun, L. Bottou, G. B. Orr, and K.-R. Müller, "Efficient backprop," in *Neural networks: Tricks of the trade*. Springer, 2012, pp. 9–48.

[24] M. R. Luo, G. Cui, and B. Rigg, "The development of the cie 2000 colour-difference formula: Ciede2000," *Color Research & Application*, vol. 26, no. 5, pp. 340–350, 2001.